Pi conjugated molecular materials themed collection – An Invitation to submit your next research to Materials Chemistry Frontiers
Electronic Properties of Tin Iodide Hybrid Perovskites: Effect of Indium Doping

SCHOLARONE™
Manuscripts

Materials Chemistry Frontiers

ARTICLE

Electronic Properties of Tin Iodide Hybrid Perovskites: Effect of Indium Doping

Keisuke Kobayashi†[b], Hiroyuki Hasegawa*‡[a], Yukihiro Takahashi[ab], Jun Harada[ab] and Tamotsu Inabe*[ab]

Indium doping is introduced to tune the electronic properties of tin iodide hybrid perovskites. By applying this method, the resistivity of tin-iodide-based hybrid perovskites is reduced using indium doping without any change in its band gap. This mixed tin/indium iodide crystal perovskite is obtained using a solution process. The resistivity of the materials continuously increased from 10^{-2} to 10^{-1} $\Omega \cdot cm$ at room temperature, even when the doping level was less than 22 ppm. The metallic nature of this system decreased with increasing doping level, while the carrier density did not vary with the doping level. This method of foreign metal doping provides resistivity control of the tin iodide hybrid cubic perovskites without changing the band gap or carrier concentration.

Introduction

The electronic structure of organic-inorganic hybrid perovskite compounds can be controlled using solution processes. Remarkable progress has been achieved for such compounds, especially for metal halide cubic perovskites for solar cells [1–11]. To enhance the efficiency of these devices, it is essential to control the electronic structure and functions of the material.

Band engineering is one method to control the electronic structure [12–14]. For example, the width of the band gap in light-emitting diodes is the dominant factor controlling the emitting wavelength; hence, the band gap of the semiconductor must correspond to the desired wavelength. The band gap of GaN corresponds to the ultraviolet region; therefore, it cannot be used as a blue-emitting diode. However, InN, which has a narrower band gap, can be used to form a mixed (In,Ga)N crystal with GaN, and the band gap can be adjusted to meet the energy for blue-light emission. This kind of band gap adjustment is available for inorganic compounds and organic-inorganic hybrid perovskites. We previously reported a method for the band gap reduction of a tin-iodide-based organic-inorganic hybrid perovskite by doping with a small amount of bismuth [15].

The parent materials of organic-inorganic tin iodide perovskites (Fig. 1) are known as not only alternative materials for lead-based perovskite solar cells [16–24] but also exceptionally conductive materials in hybrid perovskites. We reported that the highly conductive nature of these perovskites originates from the unintended spontaneous carrier doping by the Sn(IV) content [25]. A cubic crystal of $CH_3NH_3SnI_3$ exhibits metallic behavior in terms of the temperature dependencies of the conductivity and thermoelectric power even though it has a band gap of 1.3 eV. A Hall effect measurement revealed that the doping level of this material is 0.02%. Therefore, we concluded that this material is a doped semiconductor [26]. Furthermore, we demonstrated that artificial doping of Sn(IV) increased the doping level of the material. The majority carriers were holes originating from Sn(IV). This crystal can be also dedoped using a significantly excess amount of a reductant [27]. Consequently, the tin iodide perovskite has a semiconducting band structure, though the doping level depends on the sample preparation conditions.

Herein, we report another attempt of foreign metal (indium) doping into a tin iodide perovskite. As seen in indium tin oxide, indium has a good affinity with tin. In indium oxide, which is an
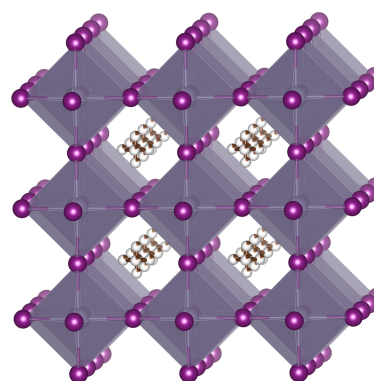
[a.] Faculty of Science, Hokkaido University, Japan. E-mail: hhase@nict.go.jp, inabe@sci.hokudai.ac.jp
[b.] Graduate School of Chemical Science and Engineering, Hokkaido University, Kita 10 Nishi 8, Kita-ku, Sapporo 060-0810, Japan
†Present address: Intellectual Property Department, Technological Affairs, Taiyo Nippon Sanso Corporation, Toyo Bldg. 1-3-26 Koyama Shinagawa-ku, Tokyo 142-8558, Japan.
‡Present address: Kobe Advanced ICT Research Institute, National Institute of Information and Communications Technology, 588-2, Iwoka, Nishi-ku, Kobe 651-2492, Japan. E-mail: hhase@nict.go.jp

Fig. 1 Cubic perovskite structure. The SnI_6 octahedra are hatched. The methylammonium cations at interstitial "A" sites are disordered.

insulator, the bottom of the conduction band consists of the 5s orbital of indium [28]. When tin atoms are doped, impurity states of Sn and voids form just below the bottom of the conduction band. In a highly doped state, these states form a band and lower the bottom of the conduction band [29–30], thereby increasing the conductivity. We present the effect of indium doping on the electronic transport, structural, and optical characteristics of tin iodide hybrid cubic perovskite bulk crystals.

Experimental details

Crystal Preparation

A previously reported procedure for preparing foreign-metal-doped cubic perovskite [15] was applied for indium doping. A stoichiometric ratio of tin(II) iodide (Kojundo Chemical Laboratory Co., Ltd.) and indium(I) iodide (Aldrich) was added to one side of an H-shaped glass tube. Methylammonium iodide was added to the other side. Then, hydroiodic acid was added separately into the tube by distillation under inert conditions. The mixture was heated to 80 °C to dissolve the metal iodides and methylammonium iodide. Then, the two solutions were mixed in the tube. Perovskite crystals were obtained as the solution slowly cooled. The chemical compositions of these crystals were determined using a Shimadzu ICPE-9000 inductively coupled plasma emission spectrometer.
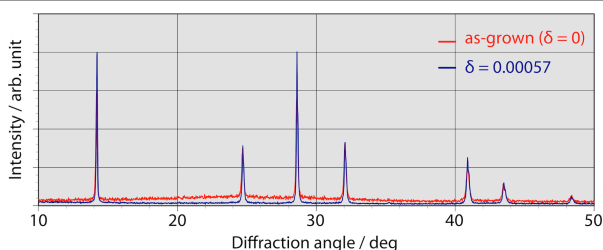

Fig. 2 Powder diffraction patterns of In-doped and as-grown (i.e., without In doping) $CH_3NH_3SnI_3$.
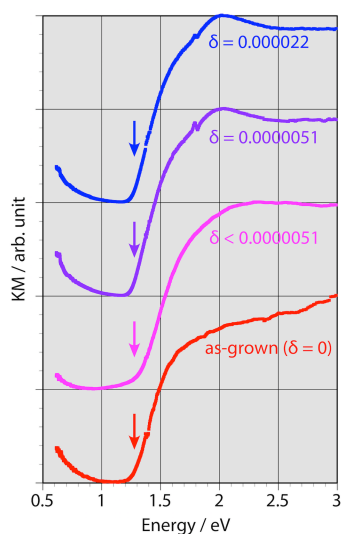

Fig. 3 Diffuse reflectance spectra of indium-doped tin iodide cubic perovskites with various amounts of doping. The arrows indicate the band gaps.

Table 1 Amount of indium doping determined by inductively coupled plasma emission spectroscopy.

Molar ratio used in sample preparation	In 0%	In 0.1%	In 1%	In 15%	In 30%
In content/%	0	ND*	0.00051	0.0022	0.0101
Sn content/%	100	-	99.99949	99.9978	99.9899
Standard deviation/%	-	-	0.00001	0.0001	<0.0001

*Below the detection limit

X-ray Diffraction

Powder X-ray diffraction data were recorded using a D8 ADVANCE diffractometer (Cu Kα radiation), and were analyzed by performing profile fitting based on the Pawley method using a TOPAS 4.2 software. All measurements were performed at room temperature.

Electronic Properties

Diffuse reflectance spectra were obtained using a JASCO V-570 UV/VIS/NIR spectrometer with an integrating sphere unit. The samples were ground with KBr. The reflectivity was converted to the Kubelka–Munk function (KM) corresponding to the absorption, and then normalized.

The temperature dependence of the conductivity was measured using a Keithley 2636A dual-channel SourceMeter. The sample was placed in a cryostat controlled by a Scientific Instruments 9700 temperature controller. The data were recorded using a custom-written software. Measurements were performed using a standard four-probe method under vacuum conditions. A carbon paste (Dotite XC-12, Fujikura Kasei Co., Ltd.) was used to mount four gold wires. The original thinner (toluene) in the carbon paste was partially evaporated by a stream of N_2 gas, and then tetralin (1,2,3,4-tetrahydronaphthalene) was added to the paste as a thinner.

Thermoelectric power measurements were performed via a method based on that reported by Chaikin and Kwak [31], using a Keithley 2182 nanovoltmeter and Advantest R6243 DC voltage current source/monitor. The samples were mounted at the gap between two gold foils using the same carbon paste used for the conductivity measurements.

Results and discussions

Indium was successfully doped into methylammonium tin iodide perovskite via an energy-saving solution process. The indium contents were determined by inductively coupled plasma emission spectroscopy. The compositional ratio of indium (δ) in the mixed crystal of $CH_3NH_3Sn_{1-\delta}In_\delta I_3$ increased upon increasing the starting molar ratio during sample preparation (Table 1); however, the efficiency of indium doping was less than that of bismuth doping [15]. There is no significant difference in chemical stability between the as-grown and the indium-doped crystals. The powder X-ray diffraction data of the doped sample indicated that the cubic structure of the tin iodide perovskite was not significantly affected by indium doping (Fig. 2). The estimated lattice parameter of the doped crystal is 6.23582(22) Å, which is almost the same as that of the as-grown
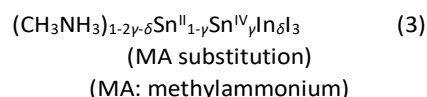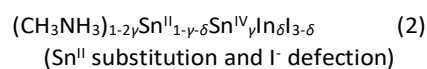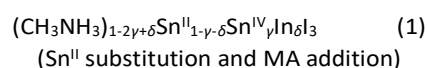
crystal (6.23176(33) Å); therefore, the basic structure of the cubic crystal was maintained.

Diffuse reflectance spectra for various indium contents (Fig. 3) revealed that the band gap of the perovskite was not affected by indium doping. As reported previously, the band gap for the as-grown crystal ($\delta = 0$) is 1.3 eV; however, there is a deviation in the near-IR region due to low-energy excitation of charge carriers [26]. The band gaps of the mixed crystals were independent of the indium doping ratios. When the influence of indium doping on the band gap is considered based on the standard electrode potential values of In and Sn (Sn/Sn^{2+}: −0.14 V, In/In^+: −0.34 V) [32–34], the 5p orbital of tin, which forms the bottom of the conduction band, has a higher potential than indium; this is consistent with our previous discussion on bismuth doping. Therefore, indium doping should lower the bottom of the conduction band. However, such an effect was not observed at any of the examined indium doping ratios. The band gap did not change within the same range of doping ratios for bismuth doping; therefore, the conduction band was not lowered because the indium content was too low.

Indium doping also affected the electronic properties. For the as-grown crystal ($\delta = 0$), the band structure was the same as that of an intrinsic semiconductor, though that is doped semiconductor due to the spontaneous doping effect. Therefore, the temperature dependence of the resistivity shows metallic behavior due to the holes injected at the top of the valence band by spontaneous doping. Fig. 4 shows the temperature dependence of the resistivity and that of the thermoelectric power for different values of δ. The resistivity increases with increasing doping ratio; metallic behavior is observed at all doping ratios. However, the slopes in the low temperature region become less steep at higher doping ratios. Sn(IV) atoms were included in the as-grown crystal ($\delta = 0$), corresponding to 0.02% holes. Doping of iodide ions can balance the electrical neutrality; otherwise, Sn(II) or methylammonium ion defects can occur. The as-grown crystal shows clear metallic behavior in terms of resistivity until low temperatures were reached; it would be more difficult to affect the crystal structure and conductivity without breaking the Sn–I framework. Therefore, the composition $(CH_3NH_3)_{1-2\gamma}Sn^{II}_{1-\gamma}Sn^{IV}_{\gamma}I_3$ with methylammonium defects is suitable here; however, the defect formation energy calculation indicates that Sn(II) defection is appropriate for the discussion of $CsSnI_3$[35].

The slopes of the thermoelectric power behaviors of the as-grown and doped crystals indicate that their Fermi levels are almost the same. Therefore, the carrier concentrations in the indium-doped crystals are also the same. Furthermore, the chemical compositions of the doped crystals change to the following compositions based on electrical neutrality:

$$(CH_3NH_3)_{1-2\gamma+\delta}Sn^{II}_{1-\gamma-\delta}Sn^{IV}_{\gamma}In_{\delta}I_3 \qquad (1)$$
$$(Sn^{II} \text{ substitution and MA addition})$$

$$(CH_3NH_3)_{1-2\gamma}Sn^{II}_{1-\gamma-\delta}Sn^{IV}_{\gamma}In_{\delta}I_{3-\delta} \qquad (2)$$
$$(Sn^{II} \text{ substitution and I}^- \text{ defection})$$

$$(CH_3NH_3)_{1-2\gamma-\delta}Sn^{II}_{1-\gamma}Sn^{IV}_{\gamma}In_{\delta}I_3 \qquad (3)$$
$$(MA \text{ substitution})$$
$$(MA: \text{ methylammonium})$$

The slope for the temperature dependence of the resistivity in the low temperature region becomes less steep with increasing indium content; this behavior differs from that reported for bismuth doping. The structural change of the Sn–I framework is closely related to the carrier conduction in the doped crystals. Thus, composition (2), which includes I$^-$ defection, is likely the appropriate composition to represent indium doping into methylammonium tin iodide perovskite at this stage. Further investigation of highly doped samples will help elucidate this situation.

Consequently, we found that indium doping reduces the conductivity without changing the band gap or carrier concentration. The mobility of the doped crystals decreased because there was no change in carrier concentration. This effect likely originates from the change in the Sn–I framework caused by indium doping.
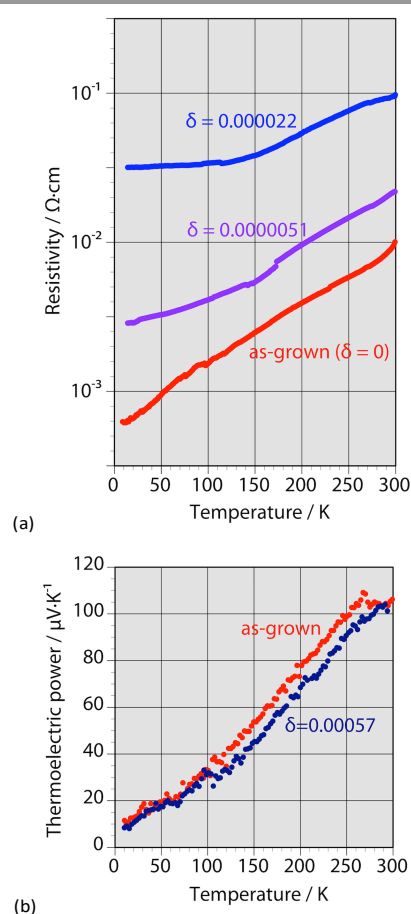

(a)

(b)

Fig. 4 (a) Temperature dependence of the resistivity of indium-doped tin iodide single crystals with various amounts of doping. (b) The temperature dependence of the thermoelectric power for the In-doped and as-grown (i.e., without In doping) $CH_3NH_3SnI_3$ single crystals.

Conclusions

For solution-processable tin iodide cubic perovskites, a small amount of indium doping reduced the conductivity without changing the band gap or the carrier concentration. In band engineering, the doped metal needs to be well matched with the parent crystal lattice to control the physical properties. However, it is difficult to predict the controllability of the physical properties by the dopant. From such a viewpoint, our research will give useful information on foreign metal doping in the hybrid perovskites. We demonstrated another possibility of foreign metal doping in tin iodide cubic perovskites and displayed a design strategy for electronic devices using hybrid perovskites, such as solar cells and light-emitting diodes. More highly efficient devices are expected to be developed using this strategy.

Conflicts of interest

There are no conflicts to declare.

Acknowledgements

Notes and references

1 A. Kojima, K. Teshima, Y. Shirai and T. Miyasaka, *J. Am. Chem. Soc.*, 2009, **131**, 6050–6051.

2 M. A. Green, A. Ho-Baillie and H. J. Snaith, *Nat. Photon.*, 2014, **8**, 506–514.

3 Y. C. Kim, K. H. Kim, D.-Y. Son, D.-N. Jeong, J.-Y. Seo, Y. S. Choi, I. T. Han, S. Y. Lee and N.-G. Park, *Nature*, 2017, **550**, 87–91.

4 H. Chen, F. Ye, W. Tang, J. He, M. Yin, Y. Wang, F. Xie, E. Bi, X. Yang, M. Grätzel and L. Han, *Nature*, 2017, **550**, 92–95.

5 Z. Ning, X. Gong, R. Comin, G. Walters, F. Fan, O. Voznyy, E. Yassitepe, A. Buin, S. Hoogland and E. H. Sargent, *Nature*, 2015, **523**, 324–328.

6 N. J. Jeon, J. H. Noh, W. S. Yang, Y. C. Kim, S. Ryu, J. Seo and S. I. Seok, *Nature*, 2015, **517**, 476–480.

7 M. Liu, M. B. Johnston and H. J. Snaith, *Nature*, 2013, **501**, 395–398.

8 W. Ke, C. C. Stoumpos, M. Zhu, L. Mao, I. Spanopoulos, J. Liu, O. Y. Kontsevoi, M. Chen, D. Sarma, Y. Zhang, M. R. Wasielewski and M. G. Kanatzidis, *Sci. Adv.*, 2017, **3**, e1701293.

9 W. Ke, C. C. Stoumpos, I. Spanopoulos, L. Mao, M. Chen, M. R. Wasielewski and M. G. Kanatzidis, *J. Am. Chem. Soc.*, 2017, **139**, 14800-14806.

10 F. O. Saouma, C. C. Stoumpos, J. Wong, M. G. Kanatzidis and J. I. Jang, *Nat. Commun.*, 2017, **8**, 742.

11 N.-G. Park, *Mater. Today*, 2015, **18**, 65–72.

12 F. Capasso, *Science*, 1987, **235**, 172-176.

13 *Band Structure Engineering in Semiconductor Microstructures*, ed. R. A. Abram and M. Jaros, Plenum Press, New York, USA, 1989, NATO ASI series. Series B, Physics; v. 189.

14 F. Withers, O. Del Pozo-Zamudio, A. Mishchenko, A. P. Rooney, A. Gholinia, K. Watanabe, T. Taniguchi, S. J. Haigh, A. K. Geim, A. I. Tartakovskii and K. S. Novoselov, *Nat. Mater.*, 2015, **14**, 301–306.

15 H. Hasegawa, K. Kobayashi, Y. Takahashi, J. Harada and T. Inabe, *J. Mater. Chem. C*, 2017, **5**, 4048–4052.

16 N. K. Noel, S. D. Stranks, A. Abate, C. Wehrenfennig, S. Guarnera, A.-A. Haghighirad, A. Sadhanala, G. E. Eperon, S. K. Pathak, M. B. Johnston, A. Petrozza, L. M. Herz and H. J. Snaith, *Energy Environ. Sci.*, 2014, **7**, 3061–3068.

17 M. H. Kumar, S. Dharani, W. L. Leong, P. P. Boix, R. R. Prabhakar, T. Baikie, C. Shi, H. Ding, R. Ramesh, M. Asta, M. Graetzel, S. G. Mhaisalkar, N. Mathews, *Adv. Mater.*, 2014. **26**, 7122–7127.

18 S. J. Lee, S. S. Shin, Y. C. Kim, D. Kim, T. K. Ahn, J. H. Noh, J. Seo, and S. I. Seok, *J. Am. Chem. Soc.*, 2016, **138**, 3974–3977.

19 Y. Zhou, Z.-J. Yong, K.-C. Zhang, B.-M. Liu, Z.-W. Wang, J.-S. Hou, Y.-Z. Fang, Y. Zhou, H.-T. Sun and B. Song, *J. Phys. Chem. Lett.*, 2016, **7**, 2735–2741.

20 J. Zhang, M.-h. Shang, P. Wang, X. Huang, J. Xu, Z. Hu, Y. Zhu and L. Han, *ACS Energy Lett.*, 2016, **1**, 535–541.

21 W. Ke, C. C. Stoumpos, I. Spanopoulos, L. Mao, M. Chen, M. R. Wasielewski and M. G. Kanatzidis, *J. Am. Chem. Soc.*, 2017, **139**, 14800–14806.

22 S. Shao, J. Liu, G. Portale, H.-H. Fang, G. R. Blake, G. H. ten Brink, L. J. A. Koster and M. A. Loi, *Adv. Energy Mater.*, 2018, **8**, 1702019.

23 S. J. Lee, S. S. Shin, J. Im, T. K. Ahn, J. H. Noh, N. J. Jeon, S. I. Seok and J. Seo, *ACS Energy Lett.*, 2018, **3**, 46–53.

24 W. Ke, P. Priyanka, S. Vegiraju, C. C. Stoumpos, I. Spanopoulos, C. M. M. Soe, T. J. Marks, M.-C. Chen and M. G. Kanatzidis, *J. Am. Chem. Soc.*, 2018, **140**, 388–393.

25 Y. Takahashi, R. Obara, Z.-Z. Lin, Y. Takahashi, T. Naito, T. Inabe, S. Ishibashi and K. Terakura, *Dalton Trans.*, 2011, **40**, 5563–5568.

26 Y. Takahashi, H. Hasegawa, Y. Takahashi and T. Inabe, *J. Solid State Chem.*, 2013, **205**, 39–43.

27 C. C. Stoumpos, C. D. Malliakas and M. G. Kanatzidis, *Inorg. Chem.*, 2013, **52**, 9019–9038.

28 J. C. C. Fan and J. B. Goodenough, *J. Appl. Phys.*, 1977, **48**, 3524–3531.

29 I. Hamberg; Ph. D. Thesis (Chalmers University of Technology, Gothenburg, Sweden, 1984)

30 H. Odaka, Y. Shigesato, T. Murakami and S. Iwata, *Jpn. J. Appl. Phys.*, 2001, **40**, 3231–3235.

31 P. M. Chaikin and J. F. Kwak, *Rev. Sci. Instrum.* 1975, **46**, 218–220.

32 *Standard Potentials in Aqueous Solution*, ed. A. J. Bard, R. Parsons, J. Jordan, Marcel Dekker, New York, USA, 1985.

33 *Encyclopedia of Electrochemistry of the Elements*, Marcel Dekker, New York, USA, 1973–1986, vol. I–IXB.

34 *CRC Handbook of Chemistry and Physics*, ed. D. R. Lide, CRC Press, Boca Raton, FL, USA, 84th edn, 2003, sect. 10.

35 I. Chung, J.-H. Song, J. Im, J. Androulakis, C. D. Malliakas, H. Li, A. J. Freeman, J. T. Kenney, and M. G. Kanatzidis, *J. Am. Chem. Soc.*, 2012, **134**, 8579–8587.